Available online at www.sciencedirect.com
SCIENCE DIRECT®
Journal of Nuclear Materials 319 (2003) 142–153
journal of nuclear materials
www.elsevier.com/locate/jnucmat

Comparison of various partial light water reactor core loadings with inert matrix and mixed-oxide fuel

U. Kasemeyer [a,*], Ch. Hellwig [b], J. Lebenhaft [b], R. Chawla [b,c]

[a] Nordostschweizerische Kraftwerke AG, CH-5312 Döttingen, Switzerland
[b] Paul Scherrer Institute, CH-5232 Villigen, PSI, Switzerland
[c] Swiss Federal Institute of Technology (EPFL), CH-1015 Lausanne, Switzerland

Abstract

Two types of plutonium-containing cores have been compared, each comprising of four different stages of plutonium deployment in an actual 1000 MW (electric) pressurized water reactor. In a first step, core-follow calculations for four real-life cores with increasingly larger mixed-oxide (MOX) loadings were validated against measured plant data. In a second step, core loadings with inert matrix fuel (IMF) have been designed and considered which contain, on the average, the same amounts of plutonium as the four partial MOX loadings. From the latter loadings, the IMF rods with the highest power ratings were identified. The data depend on a pin power reconstruction of three-dimensional nodal calculations, and a partial verification of the pin power values was carried out using the transport codes CASMO and HELIOS as well as the Monte Carlo code MCNP. Fuel behaviour calculations were then performed for the highest power-rating rods employing models partly validated via recent data from the comparatory IMF/MOX irradiation test currently under way at Halden. Based on the various results obtained, conclusions have been drawn regarding IMF rod designs most likely to yield (in partial IMF core loadings) fuel behaviour similar to that of UO_2 fuel.
© 2003 Elsevier Science B.V. All rights reserved.

1. Introduction

The world plutonium inventory is steadily growing due to the unavoidable production of plutonium in current day light water reactors (LWRs) and the de-allocation of weapon-grade plutonium from dismantled nuclear arms [1]. Accordingly, efforts are being made to increase the Pu-consumption in LWRs by using new Pu-containing inert matrix fuels (IMFs). Nowadays, mixed-oxide (MOX) fuel is widely used in LWRs in form of partial core loadings [2]. The maximum amount of MOX fuel is typically limited to about 40% of the core inventory. As a result, the plutonium consumption does not exceed the amount of plutonium which is produced from the uranium present in the core.

Usually, the amount of spent UO_2 fuel to be reprocessed after discharge from a given LWR, and hence the amount of plutonium to be brought back into the core, are fixed. Recycling the plutonium in the form of a once-through uranium-free IMF could represent a useful complementary strategy to the currently practised single recycling of plutonium as MOX. With a steadily growing number of investigations, IMFs for LWRs have been an important research topic in recent years. Thus, collaborative international efforts have led to two long-term irradiation experiments being started in 2000 [3,4]. While the irradiation test in Petten is dedicated to the investigation of different IMF concepts, that in Halden concentrates on the comparison of MOX with IMF of a particular solid-solution-type, viz. plutonium dissolved in a matrix of yttria-stabilized zirconia $(Er,Y,Pu,Zr)O_{2-x}$ [5]. It is this latter IMF concept which has been considered in the current

* Corresponding author. Tel.: +41-56 266 7732; fax: +41-56 266 7099.
E-mail address: uwe.kasemeyer@axpo.ch (U. Kasemeyer).

0022-3115/03/$ - see front matter © 2003 Elsevier Science B.V. All rights reserved.
doi:10.1016/S0022-3115(03)00146-6

comparatory investigation of partial IMF and MOX loadings in an actual 1000 MW (electric) pressurized water reactor (PWR).

For this study, a number of real-life cycles of the plant, including cycles with partial MOX loadings, have first been modelled using the Studsvik Core Management System (CMS) [6–8]. Comparisons of the calculated results with measured data in terms of the boron let-down curves and detector signal distributions showed good agreement for both UO_2 as well as MOX loadings. CMS has then been employed for investigating the behaviour of partial core loadings with IMF relative to those with MOX. The core loadings with IMF have been designed such as to contain, on the average, the same amount of plutonium as the cores with partial MOX loadings. Because there is about 50% more plutonium in IMF than in MOX fuel, these cores were loaded with about 30% less IMF assemblies than MOX assemblies and the free positions were filled with UO_2 assemblies. From these 'equivalent-plutonium' IMF loadings, the IMF rods with the highest power ratings were identified and their power history used to perform fuel behaviour calculations. Partial validation of the fuel modelling carried out in this context has been made possible via recent data from the IMF/MOX irradiation test at Halden [3]. In addition, a benchmark was set up to confirm the reliability of the pin power histories using in the fuel performance calculations. Three single assemblies fuelled with UO_2, MOX and IMF and a 3×3 lattice containing an IMF assembly surrounded by eight UO_2 assemblies were calculated with CASMO-4, SIMULATE-3, HELIOS-1.7 [9,10] and MCNPX-2.4.k (incorporating MCNP4C3) [11,12] to give a preliminary validation of the pin power reconstruction of SIMULATE.

The main points of the neutron physics and core behaviour comparisons have been the boron let-down curve (reflecting the cycle length) and the power distribution. The principal parameters compared in the fuel behaviour investigations are the fuel temperature and the fission-gas release.

2. Geometry and materials

IMF rods of different enrichments were used to reduce power peaking within the IMF assembly. A sketch of the optimized IMF assembly (similar to the used MOX assemblies) is shown in Fig. 1, with fuel rod and lattice geometry being kept the same as for UO_2 and MOX fuel.

As mentioned earlier, an actual 1000 MW (electric) PWR was modelled, the core containing 177 assemblies, arranged with a pitch of 21.56 cm and having an active core height of 358 cm. The average core conditions employed are as follows:

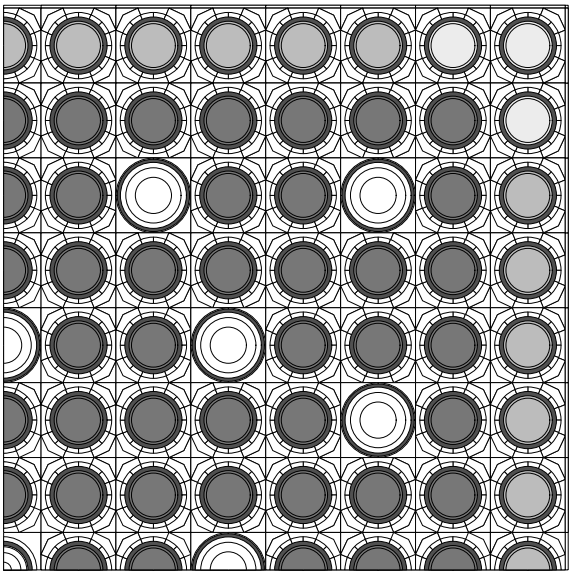

Fig. 1. Quarter-view of the IMF assembly used. (▫) Corner pins Pu/Er/Gd: 0.60/0.40/0.30 $g\,cm^{-1}$, (▪) border pins Pu/Er: 0.75/0.30 $g\,cm^{-1}$, (■) inner pins Pu/Er: 0.98/0.25 $g\,cm^{-1}$, (○) guide tube.

Total thermal power	3002 MW	Outlet temperature	598.0 K
Mean power density	102 MW m^{-3}	Water flow	15 981 kg s^{-1}
Inlet temperature	564.7 K	Pressure	15.4 MPa

3. Core-follow calculations

All calculations were done using the CASMO-4 (lattice) and SIMULATE-3 (nodal diffusion) codes of CMS [13]. The cross-section library employed was based on the JEF-2.2 data file, CMS having been earlier benchmarked with it for MOX applications [14–17]. In addition, recent neutronics measurements with IMF and MOX rodlets in a UO_2 lattice carried out in the PROTEUS facility have been analysed with CASMO-4 using the same library. Satisfactory agreement was obtained between measured and calculated power distributions for both types of Pu-fuel [5,18].

The first calculations were done for several real-life, 100% uranium-fuelled cycles. With the exception of the initial uranium cycle ('jump-in' core), all cycles showed a good agreement between measured and calculated data. Thus, for example, in all cases the root mean square (RMS) of the radial detector reaction rate distributions

was lower than 2% and the soluble boron values agreed within 30 ppm. All subsequent calculations employed UO_2 data derived for these 100% uranium cores.

4. Partial MOX core loadings

The four real-life cycles considered here with partial MOX loadings are termed MOX-1 to MOX-4. Eight MOX assemblies were loaded in cycle MOX-1, while in each of the three subsequent cycles, 20 fresh MOX assemblies were added. Four MOX assemblies, loaded in cycle MOX-3, were unloaded in cycle MOX-4, so that the latter contained a total of 64 MOX assemblies. Fig. 2 shows the comparison between measured and calculated boron let-down curves for MOX-4.

In all the partial MOX loadings, as well as in the 100% UO_2 cycles, the soluble boron values were predicted quite well at beginning of cycle (BOC), while SIMULATE underestimated the reactivity at end of cycle (EOC) by similar amounts. This behaviour was found to be independent of the cycle plutonium content and, therefore, differences reported in this paper between partial IMF and MOX loadings can clearly be attributed to differences in the burnup behaviour of the corresponding cores.

The comparison of the detector reaction rate distributions showed slightly larger spreads for the partial MOX loadings than for the 100% UO_2 cycles, the RMS being 2–3%. Considering that the detector response of the MOX assemblies is about half that of the UO_2 assemblies, this is still a good agreement between calculation and measurement.

5. Equivalent plutonium substitution with IMF assemblies

Core loadings with IMF have been designed which contain, on average, the same amount of plutonium as the cores considered with partial MOX loadings. Because of the core quarter-symmetry, the number of loaded fresh assemblies should be divisible by four. Eight IMF assemblies were loaded in the first cycle, while in each of the three following cycles 12 fresh IMF assemblies (instead of 20 MOX assemblies) were loaded so that the fourth cycle contained 44 IMF assemblies. The remaining MOX assembly positions were filled with UO_2 fuel. While the core design of the first core was the same as in the previous case, the loading schemes for the other three cores were adjusted to yield a maximum relative radial nodal power of about 1.5 and maximum IMF pin power values of about 420 $W\,cm^{-1}$.

The reactivity at EOC could be increased in each case, except for the first partial IMF core. This can be seen in Fig. 3 which compares the boron let-down curves for the fourth cycle with partial MOX and IMF loadings. In the present calculations, the cycle length in all cases was in fact kept the same as in the original MOX cores and no additional burnup was accumulated. The advantage, however, was that fewer fresh UO_2 assemblies needed to be loaded to get the same cycle length. If additional burnup had been aimed at, the cycle length could have been increased by about 20, 40 and 25 EFPD, respectively, for the considered second, third and fourth cycles with partial IMF loadings.

As mentioned above, the maximum relative radial nodal power fraction was adjusted in each core with

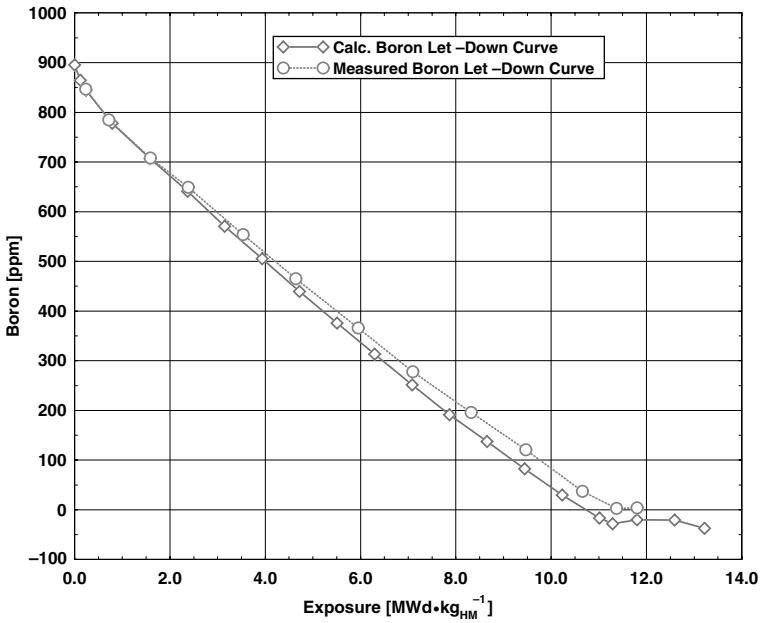

Fig. 2. Comparison between measured and calculated boron let-down curves for cycle MOX-4.

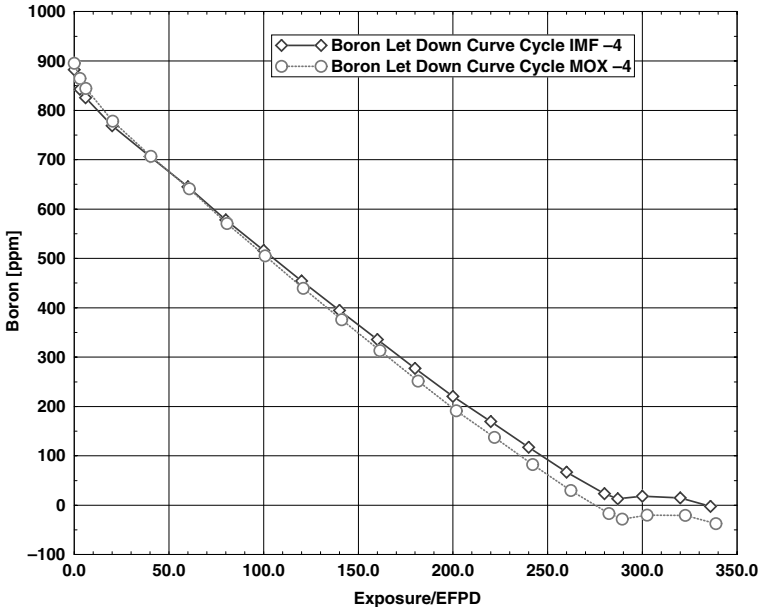

Fig. 3. Comparison between boron let-down curves of the fourth core with equivalent plutonium (44 IMF, 64 MOX assemblies).

partial IMF loading to be about 1.5. The highest relative radial power fractions were found at BOC in the third cycle. Fig. 4 shows the comparison between partial MOX and IMF loadings in this particular case.

The highest pin power value of a UO_2 fuel rod was found to be 512 $W\,cm^{-1}$, while the maximum value for an IMF rod was 434 $W\,cm^{-1}$. The axially averaged pin power histories of the hottest UO_2 and IMF rods were

0.985 0.975 1.051	1.304 1.301 0.225	1.256 1.079 16.401	0.863 1.471 -41.295	1.067 1.274 -16.217	0.993 1.001 -0.794	1.526 1.419 7.518	0.455 0.399 14.064
1.303 1.299 0.265	1.336 1.253 6.645	1.296 1.284 0.960	1.073 1.090 -1.550	0.867 1.416 -38.788	1.087 1.118 -2.811	1.481 1.293 14.513	0.428 0.343 25.069
1.257 1.079 16.547	1.300 1.284 1.270	1.268 1.280 -0.931	0.958 1.446 -33.776	1.207 1.078 11.907	1.242 1.149 8.061	1.271 0.828 53.458	0.296 0.218 35.816
0.867 1.470 -41.074	1.084 1.091 -0.706	0.966 1.445 -33.165	1.202 1.256 -4.323	1.324 1.063 24.549	1.433 1.348 6.336	0.494 0.430 14.664	
1.066 1.273 -16.278	0.875 1.415 -38.161	1.217 1.070 13.675	1.337 1.062 25.966	1.519 1.477 2.843	0.684 0.880 -22.257	0.227 0.240 -5.491	
0.988 1.001 -1.254	1.098 1.119 -1.932	1.282 1.157 10.817	1.461 1.349 8.365	0.691 0.881 -21.491	0.260 0.303 -14.268		
1.523 1.419 7.353	1.500 1.304 14.991	1.307 0.851 53.634	0.520 0.425 22.343	0.232 0.240 -3.605			
0.454 0.399 13.925	0.436 0.347 25.569	0.304 0.221 37.402	IMF MOX %-Diff.				

Fig. 4. Comparison between relative power distributions at BOC in the third core with 32 IMF (1st line) and 44 MOX (2nd line) assemblies.

used to investigate fuel behaviour characteristics using an extended version of the fuel performance code TRANSURANUS [19,20].

5.1. Plutonium reduction

Comparing the effectiveness of the two different equivalent-Pu strategies in terms of plutonium reduction, one finds that around 15 of the initial plutonium remains in the discharged MOX assemblies, while in the case of an IMF assembly the corresponding fraction is only 2/5. Table 1 summarizes the results for the plutonium consumption achieved with IMF and MOX fuel.

On average, 16 MOX or 11 IMF assemblies would be discharged at each stage of an equilibrium cycle. Hence, about 167 kg plutonium would be destroyed by using MOX, while 284 kg plutonium would be destroyed with the use of IMF. Table 2 summarizes the overall plutonium balance (i.e. including the UO_2 assemblies) for a single equilibrium cycle stage. It is seen thereby that the plutonium consumption of a core with a partial IMF loading would be four times as large as that in the corresponding case with MOX.

Table 1
Fractions (wt%) of initial plutonium remaining at discharge and the total-destroyed plutonium amounts for the two considered fuel types

Case	Pu_{tot}	Pu_{fiss}	Destroyed Pu
	Weight of initial Pu (%)		Mass per assembly (kg)
MOX	66.2	35.7	10.4
IMF	41.2	16.4	25.8

Table 2
Comparison of overall plutonium balances with partial MOX and IMF loadings for a single equilibrium cycle stage

	MOX	IMF
Loaded Pu[a]	493	483
Discharged Pu[b]	462	359
Pu balance	−31	−124

All values are given in kg.
[a] Pu in 16 MOX or 11 IMF assemblies.
[b] Pu in 44.25 discharged assemblies (on average).

6. Benchmarking of the pin power results

Before reporting on the fuel behaviour study, a partial validation of the pin power reconstruction methodology used is presented in this section. This methodology, viz. that employed by the three-dimensional nodal code SIMULATE-3, is based on pin power distributions calculated by the lattice code CASMO-4 for a single assembly. According, the pin data of CASMO-4 (and the pin and nodal data of SIMULATE-3) have been compared, for four different reference cases, against benchmark results obtained using HELIOS-1.7 and MCNPX. The first three cases are single fuel assemblies loaded with UO_2, MOX and IMF. The fourth calculated case is a lattice of 3×3 fuel assemblies, representing a partial IMF loading, viz. a central IMF assembly surrounded by eight UO_2 assemblies. All cases were calculated for xenon-free conditions at cold zero power ($T_{fuel} = T_{clad} = T_{modr} = 300$ K) and at hot full power (HFP) (($T_{fuel} = 1000/1500$ K, $T_{clad} = T_{modr} = 560$ K). Other temperatures were not considered because of limited MCNP libraries.

All single assembly calculations were performed using CASMO-4, HELIOS-1.7 and MCNPX-2.4.k (which incorporates MCNP4C3), while in the 3×3 case SIMULATE-3 was used instead of CASMO-4. The cross-section libraries employed were based on the JEF-2.2 nuclear data evaluation for CASMO and on ENDF/B-VI for HELIOS. The continuous-energy MCNP calculations were carried out using both libraries. For each case and temperature condition, comparison have been made of k_∞ and the assembly relative pin power values obtained with the different codes.

6.1. Results of the comparisons

The results of the inter-code comparisons for the k_∞ predictions are shown in Table 3. Because the relative

Table 3
Comparison of k_∞ of the various cases for hot conditions calculated with CASMO, HELIOS, MCNP and SIMULATE

Code	Library	Case I, UO_2 single FA	Case II, MOX single FA	Case III, IMF single FA	Case IV, 3×3 with IMF
CASMO	JEF-2.2	1.4212	1.1910	1.0801	–
MCNP	JEF-2.2	1.4266	1.1824	1.0704	1.3489
HELIOS	ENDF/B-6	1.4157	1.1775	1.0667	1.3392
MCNP	ENDF/B-6	1.4221	1.1812	1.0717	1.3442
SIMULATE	JEF-2.2	–	–	–	1.3413
Average	–	1.4214	1.1830	1.0722	1.3432

Statistical 1σ-errors for MCNP are all smaller than 0.3 mk.

differences between results for the cold and the hot cases were found to be very similar, only the comparisons for the hot cases are shown here.

In most cases, the k_∞ of the different codes agrees within a few mk. The largest differences can be seen in the Pu-cases between CASMO and HELIOS, while the MCNP predictions generally agree with the average value quite well. Relative to the average results, CASMO overestimates k_∞, especially in the plutonium cases, while HELIOS underpredicts the eigenvalue each time. This indicates that CASMO and SIMULATE are likely to overpredict the power in plutonium containing assemblies.

The relative pin power distributions in the single assemblies have been compared by normalizing results obtained with each of the deterministic codes to MCNP results in each case. Because of the excellent agreement for the UO_2 and MOX cases, the comparisons are presented only for the hot IMF calculations. Tables 4 and 5 give the results.

The comparisons of the pin power values indicate that CASMO overestimates the power of the corner pins. In comparison with the MCNP calculation based on the JEF-2.2 library, CASMO predicts up to about 5% higher power while HELIOS underpredicts the power by up to 2.4% in comparison to the MCNP prediction with the ENDF/B-6 library. Overall, the comparisons between HELIOS and MCNP show good agreement with differences of typically 1%. Because the corner pins, in partial IMF loadings, will see the highest thermal flux, an overprediction of the power within these pins such as with CASMO will result in conservative results for the fuel behaviour calculations.

The 3×3 fuel assembly configuration representing a partial IMF loading was investigated with a two-dimensional SIMULATE model and compared with HELIOS and MCNP results. Table 6 shows the ratios of the relative assembly-average power distributions in the 3×3 lattice between SIMULATE and HELIOS on the left, and SIMULATE and MCNP on the right.

These results indicate that the IMF assembly power is overpredicted with SIMULATE, while the power of the UO_2 assemblies is slightly too low. This means that at BOC in the core-follow calculations, the nodal power of the UO_2 is also slightly underestimated while the power in the fresh IMF assemblies is too high. A validation for cases with burnup will be the subject of further studies.

The last comparison within this validation investigation was made for the relative pin power distribution in the IMF assembly of the 3×3 lattice. Tables 7 and 8 show the ratios between SIMULATE and MCNP, and between HELIOS and MCNP predictions of the relative pin powers.

The SIMULATE pin power distribution for the IMF assembly in the 3×3 lattice resembles that obtained with

Table 4
Ratio of pin power values in the hot IMF assembly between CASMO and MCNP with JEF-2.2

–							
0.993	1.011						
0.985	0.994	1.011					
–	0.988	0.988	–				
0.991	0.998	0.986	0.978	1.004			
0.994	0.995	–	0.985	0.997	–		
1.006	0.999	0.987	0.997	1.007	1.004	1.050	
1.021	1.013	1.023	1.022	1.026	1.049	1.015	1.040[a]

Statistical 1σ-errors for MCNP are all smaller than 1.0%.
[a] South-east corner of the assembly.

Table 5
Ratio of pin power values in the hot IMF assembly between HELIOS and MCNP with ENDF/B-6

–							
0.986	1.009						
0.996	1.006	0.995					
–	1.000	0.987	–				
0.985	1.006	0.998	0.989	1.001			
1.001	0.997	–	0.994	0.988	–		
1.005	1.014	0.999	0.994	1.007	0.983	0.996	
1.006	1.007	1.006	1.002	0.999	0.989	0.976	0.980[a]

Statistical 1σ-errors for MCNP are all smaller than 1.0%.
[a] South-east corner of the assembly.

Table 6
Ratio of assembly-average power values in the 3×3 lattice between SIMULATE and HELIOS (left side) and between SIMULATE and MCNP (right side)

0.991	0.999	0.991
0.999	1.060	0.999
0.991	0.999	0.991

0.991	1.001	0.991
1.001	1.054	1.001
0.991	1.001	0.991

Statistical 1σ-errors for MCNP are all smaller than 0.5%.

CASMO for the single IMF assembly. In particular, the power of the second row corner pin is seen to be overestimated by approximately 7%. Apart from the corner pins, the differences between SIMULATE and MCNP are usually less than 5.0%. The differences for the corner pins appear to result from the pin power reconstruction, based on the single-assembly pin power calculated by CASMO. Thus, all in all, the IMF pin power histories obtained with SIMULATE, which have been used in the fuel behaviour assessment described in the next section, can be called conservative.

The agreement between HELIOS and MCNP is also good in the 3×3 case, the differences between the codes being largely within the range of the statistical errors of the MCNP calculations. This provides some confidence in the analysis of the Halden irradiation test IFA-651, which is also based on HELIOS calculations. Furthermore, the present results indicate that HELIOS can be used for further validation studies of nodal calculations with burnup.

7. Comparison between IMF and UO_2 fuel behaviour

To permit the modelling of the fuel performance of IMF, the TRANSURANUS code has been modified by PSI for this new type of fuel [21]. This was done using the following material data for yttria-stabilized zirconia or – if available – for the fabricated fuel: thermal expansion, yield stress, Young's modulus, emissivity, melting temperature, specific heat and density. Since no data have been found for a creep strain correlation for yttria-stabilized zirconia, the UO_2 correlation was adopted for IMF (the creep strain correlation is of

Table 7
Ratios of relative pin power in the IMF assembly of the 3×3 lattice between SIMULATE and MCNP

–							
1.049	1.054						
1.041	1.040	1.030					
–	1.009	0.996	–				
1.029	1.023	1.009	1.008	1.002			
1.027	1.012	–	1.005	0.991	–		
0.989	0.995	0.994	0.989	0.997	1.000	1.068	
0.970	0.971	0.961	0.973	0.977	0.981	1.005	1.031[a]

Statistical 1σ-errors for MCNP are all smaller than 1.0%.
[a] South-east corner of the assembly.

Table 8
Ratios of relative pin power in the IMF assembly of the 3×3 lattice between HELIOS and MCNP

–							
0.982	1.013						
0.983	1.005	1.024					
–	0.995	0.991	–				
1.001	1.010	1.003	1.003	1.008			
1.012	0.999	–	0.984	0.999	–		
1.013	1.013	1.006	0.997	1.016	1.007	1.010	
0.999	1.008	0.996	0.998	1.001	1.008	0.983	0.969[a]

All errors in the MCNP calculation are smaller than 1.0%.
[a] South-east corner of the assembly.

relatively minor importance for the calculations). The thermal conductivity was derived from measurements carried out with fuel samples at ITU, Karlsruhe, up to temperatures of 1893 K.

There is not enough data currently available to establish a fission gas release behaviour model for IMF. Nevertheless, there are indications from the Halden irradiation test, as well as from other related experiments, that the fission gas release behaviour could be quite similar to that of UO_2. Therefore, the same model has been used for IMF. Other models for fuel irradiation behaviour (relocation, swelling, densification) have been adjusted to fit the in-pile data recently made available from Halden. As only three IMF rods (with slightly different design and instrumentation) are being irradiated in this test, and the burnup achieved till now is only about 4.5 MWd kg^{-1} (MOX-equivalent burnup), the validation base for the chosen assumptions is rather limited. The calculational results currently reported should not, therefore, be viewed as accurate predictions of IMF behaviour, but rather as a contribution to fuel rod design optimization on the basis of the irradiation data available to date.

7.1. Pin power histories

The CMS-calculated power histories for the hottest IMF rod and the hottest UO_2 rod, as well as the corresponding axial profiles, have been used as input in TRANSURANUS (each rod was virtually divided into 20 axial slices for calculation). The power histories employed are given in Table 9, the differences indicated being essentially due to the use of a burnable absorber and the absence of any plutonium production in the case of IMF. Because an axially averaged pin power history from CMS was used in TRANURANUS a slightly lower peak-power than calculated with CMS has been used for the hottest IMF rod by TRANURANUS.

The power history of the UO_2 rod decreases steadily from each BOC to EOC. The power history of the IMF rod increases first, due to Gd-consumption and then shows a turn-around after 80 days in the second cycle.

7.2. Geometrical input data

The geometry of the cladding of the IMF rod was the same as in the UO_2 case. The design of the pellets was modified in two respects. Firstly, the pellet outer diameter was slightly increased, i.e. the gap size slightly decreased, in accordance with the different (reduced) swelling and relocation behaviour of IMF observed in the Halden experiment. Secondly, a central hole of 3 mm diameter was introduced in order to lower the fuel centre temperature. For comparison reasons, a calculation was also done for an IMF rod without a central hole. It should be mentioned that the hole diameter was not optimized, but was rather a compromise between fabrication feasibility (the hole should be fabricated by pressing, not drilling) and residual pellet mass. The pellet mass decreases just by 11%, so that the plutonium content of the IMF needs to be enhanced only by this amount to achieve the same power generation. Such a moderately higher plutonium content is not expected to alter the material properties of this IMF-type significantly.

7.3. Results of the fuel behaviour calculations

Various results of the TRANSURANUS calculations for the UO_2 and IMF rods are presented in Tables 10 and 11. Graphical representations of the main results as function of burnup are given in Figs. 5 and 6.

The hottest UO_2 rod nearly reaches the specified limiting fuel centre temperature according to the present calculations. The gap closes during the first cycle in most

Table 9
Simplified power histories for the hottest rods, UO_2 and IMF, used as input for TRANSURANUS

	UO_2 peak power (kW m^{-1})	UO_2 average power (kW m^{-1})	IMF peak power (kW m^{-1})	IMF average power (kW m^{-1})
BOC 1	49.7	40.0	23.7	19.9
EOC 1	37.2	34.4	37.7	32.0
BOC 2	42.2	34.4	40.2	33.7
After 80 EFPD		Interpolation	41.5	35.6
EOC 2	30.6	28.0	33.1	32.3
BOC 3	34.8	28.0	24.0	20.1
EOC 3	24.0	22.0	18.5	15.7
BOC 4	27.3	22.0	17.9	15.0
EOC 4	17.5	16.0	16.5	14.0

Table 10
TRANSURANUS results for the hottest pins at end of irradiation and under HFP conditions

	UO_2 rod	IMF rod (annular pellet)	IMF rod (full pellet)
Average rod burnup [MWd kg^{-1}][a]	60.7	56.3[b]	50.4[b]
Maximum/average fuel temperature [K]	1215/913	911/862	1427/952
Fission gas production [cm^3]	4134	3514	3511
Fission gas release [cm^3/%]	431/10.4	458/13.0	717/20.4
Hot/cold plenum pressure [MPa]	11.6/4.4	9.4/3.3	13.0/5.1

[a] Reported for heavy metal.
[b] MOX-equivalent burnup.

Table 11
Maximum values of various parameters during irradiation

	Specification limit (UO_2)	UO_2 rod	IMF rod (annular pellet)	IMF rod (full pellet)
Fuel centre temperature [K]	2278	2194	1920	2378
Average fuel temperature [K]	–	1268	1262	1407
Time of maximum value	–	BOC of 1st cycle	After 80 EFPD of 2nd cycle	
Fuel outer temperature [K]	826	822	712	756
Clad inner temperature [K]	–	662	676	678
Clad outer temperature [K]	620	622	622	622
Coolant temperature[a] [K]	617	617	617	617
Rod pressure [MPa]	–	12.4	10.1	14.1

[a] Coolant outlet temperature in hottest channel limited by boiling point at operational pressure of 15.4 MPa.

of the slices. In the hotter slices (slices 5–14), cladding lift-off can be observed during the fourth cycle. The rod inner pressure is slightly reduced by this cladding lift-off, while the fuel axial deformation is decoupled from the clad axial deformation. The relative fission gas release has its peak value during the second cycle. After that, it is decreasing due to the steadily increasing amount of produced fission gas.

The hottest IMF rod (annular pellet) reaches its maximum temperature after 80 days of the second cycle due to the corresponding power history (as mentioned earlier, this peak is caused by the consumption of the burnable poison). The gap closes, also in this case, during the first cycle for most of the slices. There are no signs of cladding lift-off later. The greater free volume due to the central hole is more than sufficient to compensate for the increased fission gas release, compared to UO_2. The fuel axial deformation is significantly smaller than found for UO_2. It is reduced by the strong IMF resintering, observed in the Halden test, as well as by the modified (i.e. strongly reduced) swelling model for IMF. The fission gas release in the IMF rod is higher than in the UO_2 rod despite the lower fuel centre temperature. This can be explained by the lower thermal conductivity and the different radial power profile resulting in a temperature profile with a larger fuel volume at higher temperatures. The larger fuel volume (in the IMF case) which runs at elevated temperatures triggers fission gas release.

7.4. Discussion of fuel behaviour modelling results

Although relatively large uncertainties are associated with the use of the current models for IMF (based largely on yttria-stabilized zirconia), this first set of modelling results delivers useful information pertaining to the technical feasibility of this new fuel type. It indeed appears possible to employ Pu–Er–Zr oxide as IMF in a current-day PWR. The introduction of a central hole seems necessary in the fuel rod design to avoid too high fuel center temperatures. However, if the maximum power would be decreased by 5–10%, further core design optimization could even permit the use of full IMF pellets.

The present uncertainties associated with the fission gas release model for IMF are particularly significant. However, as the gap is closed in the hot axial region, there is little effect of these uncertainties on the maximum fuel temperature. Their influence on the rod inner pressure is somewhat compensated by the larger free volume resulting from the central hole. The large uncertainties associated with the swelling model have negligible influence on the thermal behaviour of the IMF rod.

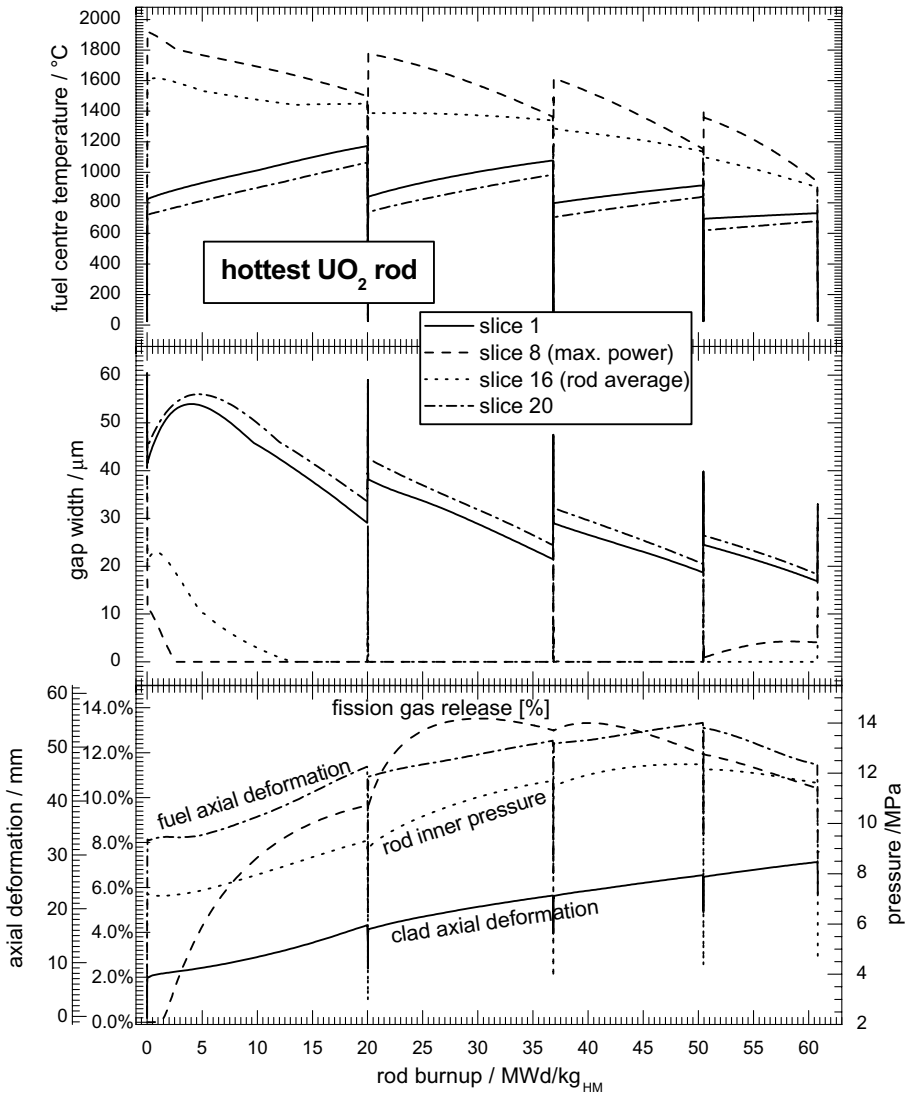

Fig. 5. Graphical representations of the main modelling results for the hottest UO_2 rod.

8. Conclusions

From the current investigations, the following conclusions can be drawn:

- A clear reduction in the number of required Pu-fuel assemblies is possible with IMF.
- An equivalent-Pu replacement of MOX assemblies in a 36% partial loading by IMF (and UO_2) assemblies is possible with simple core optimization and yields in benefits of a four times larger, overall plutonium reduction and possible better use of UO_2 fuel due to the resulting longer cycle length.
- Partial loadings with higher fractions of IMF assemblies appear to be more difficult due to the increased power peaking which results in the UO_2 assemblies.
- The preliminary assessment of the pin power reconstruction with SIMULATE has indicated that the relative nodal power of IMF assemblies in partial loadings, as well as the pin powers of the corner pins in such assemblies, are overestimated. This can be expected to lead to too high peaking power for the power history of the IMF rods with the highest power ratings, and hence to more conservative results of the fuel performance calculations.
- Such conservative, fuel performance calculations for an annular IMF rod design delivered results within currently specified limits for UO_2.

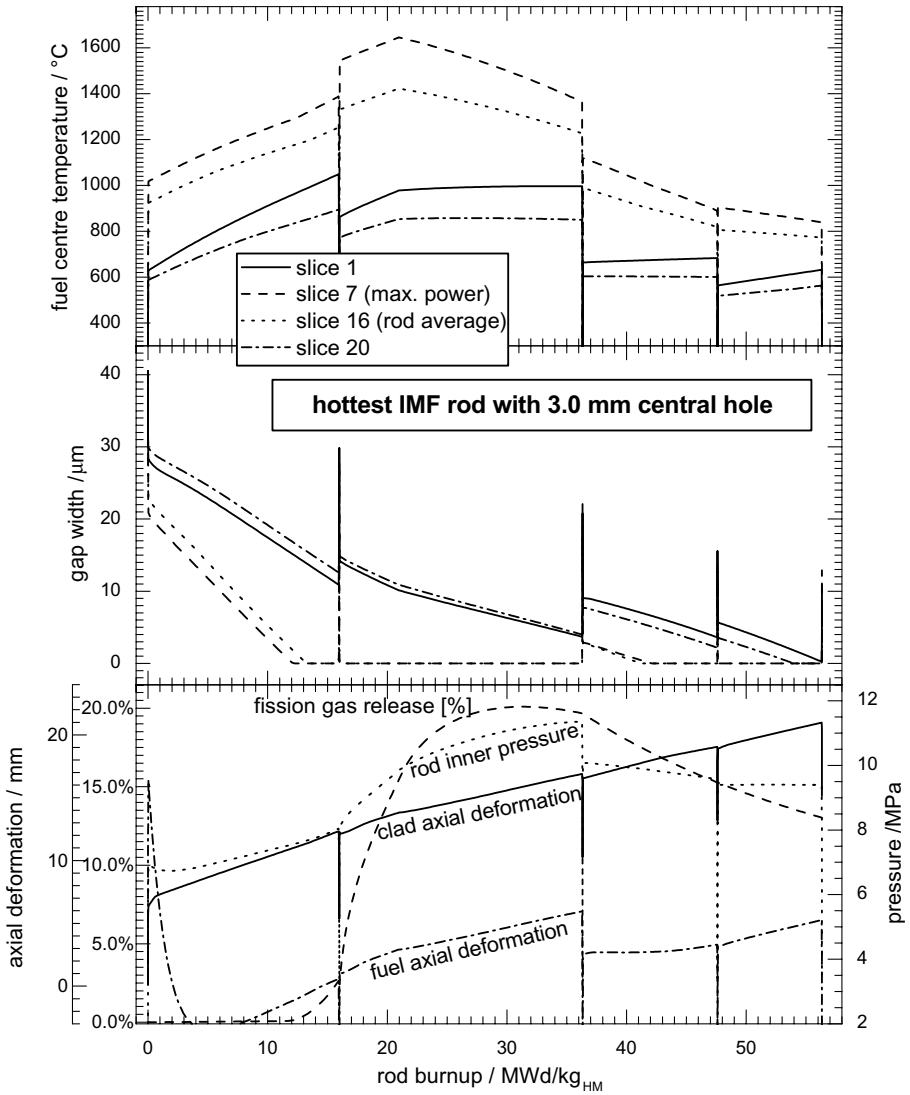

Fig. 6. Graphical representations of the main modelling results for the hottest IMF rod (burnup equivalent to MOX).

- Maximum fuel centre temperature in the case of full IMF pellets is about 100 K above the limit specified for UO_2 but could be lowered by further core design optimization.
- The relatively large, present uncertainties in fission gas release and fuel swelling models for IMF should not significantly influence the reported maximum fuel temperature results. Further data from the ongoing IMF irradiation test at Halden, of course, remain crucial.

References

[1] J.-S. Choi, IAEA, in: N. Numark, A. Michel (Eds.), Proceedings of the Conference Report of the International Conference on the Future of Plutonium, October 2000, Brussels, Belgium.

[2] P. Ledermann, D. Grenèche, in: Proceedings of the International Conference on Future Nuclear Systems GLOBAL'99, August–September 1999, Jackson Hole, Wyoming, USA.

[3] U. Kasemeyer, Ch. Hellwig, Y.-W. Lee, G. Ledergerber, D.S. Sohn, G.A. Gates, W. Wiesenack, Prog. Nucl. Energy 383&384 (2001) 309.

[4] R.P.C. Schram, K. Bakker, H. Hein, J.G. Boshoven, R.R. van der Laan, T. Yamashita, G. Ledergerber, F. Ingold, Prog. Nucl. Energy 383&384 (2001) 259.

[5] R. Chawla, C. Hellwig, F. Jatuff, U. Kasemeyer, G. Ledergerber, B.H. Lee, G. Rossiter, in: Proceedings of the ENS TOPFUEL 2001, Stockholm, Sweden, 27–30 May 2001.

[6] M. Edenius, K. Ekberg, B.H. Forssen, D. Knott, CASMO-4, a Fuel Assembly Burnup Program, User's Manual, StudsvikSOA-951, Studsvik of America, Newton MA, September 1995.
[7] J.J. Casal, R.J.J. Stamm'ler, E.A. Villarino, A.A. Ferri, in: Proceedings of the International Topical Meeting on Advances in Mathematics, Computations and Reactor Physics, vol. 2, Pittsburgh, USA, 1991, p. 10.2.1.
[8] E.A. Villarino, R.J.J. Stamm'ler, in: Proceedings of the International Conference on Physics of Reactors PHYSOR 96, Mito, Japan, September 1996, vol. 1, p. A230.
[9] J.F. Briesmeister (Ed.), MCNP-A General Monte Carlo N-Particle Transport Code, Version 4C, Los Alamos National Laboratory, LA-13709-M, April 2000.
[10] L.S. Waters, MCNPX User's Manual, Version 2.3.0, Los Alamos National Laboratory, LA-UR-02-2607, April 2002.
[11] T. Bahadir, CMS-Link User's Manual, StudsvikSOA-9704, Studsvik of America, Newton MA, 1997.
[12] A.S. DiGiovine, J.D. Rhodes, SIMULATE-3 User's Manual, StudsvikSOA-9515, Studsvik of America, Newton MA, 1995.
[13] M. Edenius et al., Core Analysis: New Features and Applications, Nuclear Europe Worldscan, No. 3/4, March–April, 1995, p. 35.
[14] M. Edenius, D. Knott, K. Smith, in: Proceedings of the International Conference on Physics of Nuclear Science and Technology, vol. 1, Long Island, NY, October 1998, p. 135.
[15] D. Knott et al., in: Proceedings of the International Conference on Physics of Nuclear Science and Technology, vol. 1, Long Island, NY, October 1998, p. 51.
[16] M. Edenius, D. Knott, K. Smith, Technical Meeting of Fuel Assembly and Reactor Physics and Calculation Methods Groups of the German Nuclear Society (KTG), Karlsruhe, Germany, February 1998, p. 27.
[17] M. Mori, M. Kawamura, K. Yamate, Nucl. Sci. Eng. 121 (1995) 41.
[18] R. Chawla, P. Grimm, P. Heimgartner, F. Jatuff, G. Ledergerber, A. Lüthi, M. Murphy, R. Seiler, R. van Geemert, Prog. Nucl. Energy 38 (2001) 359.
[19] K. Lassmann, J. Nucl. Mater. 188 (1992) 295.
[20] K. Lassmann, A. Schubert, J. van de Laar, C.W.H.M. Vennix, Recent developments of the TRANSURANUS code with emphasis on high burnup phenomena, IAEA Technical Committee Meeting on Nuclear Fuel Behaviour Modelling at High Burnup, Lake Windermere, UK, June 2000.
[21] Ch. Hellwig, U. Kasemeyer, in: Proceedings of the Enlarged Halden Group Meeting, March 2001, Lillehammer, Norway.